**Supplementary Material for:**

# Pressure and Temperature Dependences of Rate Coefficients for the Reaction OH + $NO_2$ + M → Products

Frank A. F. Winiberg[1], Kristen Zuraski[1], Yingdi Liu[1,2], Stanley P. Sander[1] and Carl J. Percival[1*]

[1] NASA Jet Propulsion Laboratory, California Institute of Technology, Pasadena, CA, USA

[2] SRI International, Menlo Park, CA USA;

***Corresponding Author**

Carl J. Percival, Phone: 1-818-354-5581, E-mail: carl.j.percival@jpl.nasa.gov

## Contents



16 Pages

12 Figures

## 1 Pre-cooled inlet

The Pulsed Laser Photolysis, Laser Induced Fluorescence (PLP-LIF) maintains the gas temperature in the reaction zone through an internally cooled copper "shroud". By flowing cold methanol through the shroud, the cell was able to reach temperatures as low as ~235 K, however cooling room temperature gas was inefficient and limited by the freezing point of methanol (~195 K). The PLP-LIF apparatus was augmented with a pre-cooled inlet (Figure S 1) which was designed to pre-cool the gas mixture up to the internal copper shroud inside the chamber. The inlet is a glass jacket design, ~1.5" O.D., ~0.86" I.D. and 18" long. Mounted on the reactor using a 1.5" o-ring sealed ConFlat flange (2.75" flange diameter), the jacket extends passed the chamber wall, sitting flush with the internal cooling shroud. The internal 1" O.D. tube extends past the copper shroud to ensure cold gas delivered directly into the reaction volume.

The coolant was introduced to the front of the cooling jacket via a ¼" glass tube mounted inside the jacket. This ensured that coolant was distributed more evenly across the entire length of the inlet. Coolant was passed through the chamber's internal cooling shroud before entering the cooled inlet.

Whilst previous experiments have shown the capability of the PLP-LIF to reach temperatures close to ~190 K (Liu and Sander, 2015), the inlet has dramatically improved the stability of the temperatures <250 K to within ±1 K, along with the ease of reaching stable colder set-points (220 K in ~1.5 hours versus 4 – 5 hours previously). Additionally, temperature profile measurements showed a small deviation in the temperature of ±2 K across the entire inlet and reaction region.

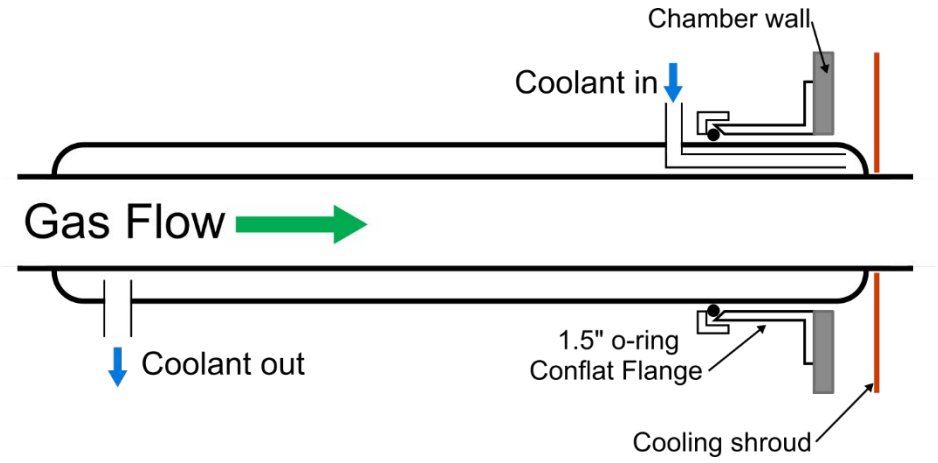


Figure S 1: Diagram of the pre-cooled inlet with respect to the reactor wall and internal cooling shroud (not to scale). The cooled inlet allows cold gas to be injected directly to the reaction volume.

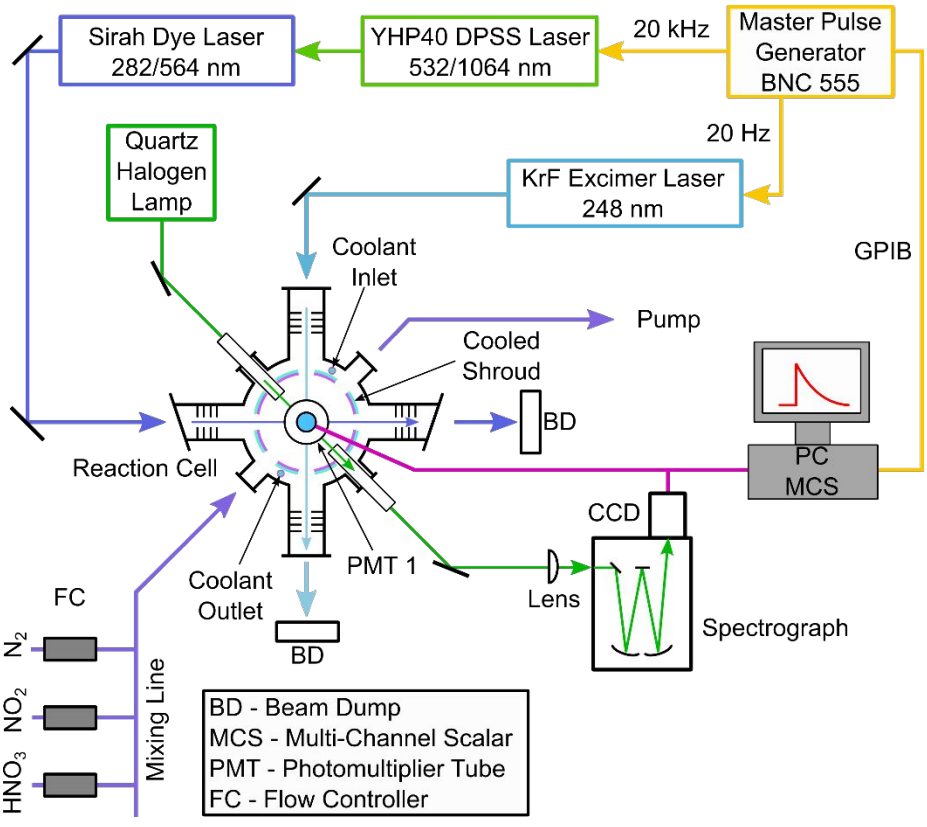


Figure S 2: Schematic of the PLP-LIF apparatus used in the study of OH + $NO_2$.

## 2 Reanalysis of Mollner et al. (2010) data

Datasets were reanalyzed corresponding to the data presented in the Mollner et al. (2010) publication taken in $N_2$ at 298 K. Raw data was reanalyzed using the $NO_2$ cross section data from Nizkorodov et al. (2004) and the fitting routine used to determine [$NO_2$] in the current study. Raw OH LIF decays were also reanalyzed to generate bi-molecular plots (example at 200 Torr $N_2$ shown in Figure S 3). The reanalyzed data was observed to be within ~4% of the data presented in Mollner et al. (2010); well within the experimental uncertainty and most likely due to the slight difference in the absorption cross sections used (discussion below).

By examining the $NO_2$ cross section used in this study (Nizkorodov et al., 2004) compared to that retrieved from the Mollner et al. (2010) data analysis files and the Vandaele et al. (2002) absorption cross section used in the recent kinetic study by Amedro et al. (2019), it can clearly be seen in Figure S 4 that the cross sections are in excellent agreement. The absorption cross sections from Mollner et al. (2010) and Vandaele et al. (2002) are within their respective quoted uncertainties (3.6 and 7% (±2σ)).

The spectrum used by Mollner et al. (2010) is presented as found in the analysis files, however the Vandaele et al. (2002) and Nizkorodov et al. (2004) spectra are convolved with the instrument line shape (ILS) used in the current study, defined by a Gaussian with a FWHM = 0.2 nm, and a pressure dependent Lorentzian function ($\lambda_{center}$ = 425 nm, Full Width Half Max (FWHM) ~0.002 nm). Integrated areas for the Gaussian and Lorentzian function were normalized to a total of 1 before convolution. It should be noted that the experimental setup used in this work and Mollner et al. (2010) is almost identical. Mollner et al. (2010) measured $NO_2$ with a single pass UV-Vis setup, a different CCD array and likely different spectrograph slit widths (these were not recorded with the datafiles); despite this we do not expect any significant differences in the ILS.

The Nizkorodov et al. (2004) cross section used in this work (recorded at 0.99 Torr) was convolved with a Lorentzian line shape parameter representative of pressure broadening at 760 Torr, as described in Nizkorodov et al. (2004). Applying a Lorentzian line shape broadening factor has been demonstrated to have negligible effect on the convolved spectrum compared to the ILS (Amedro et al., 2019; Winiberg, 2019). Both datasets shown in Figure S 5 are visually indistinguishable and a linear regression comparing the two datasets in this spectral window yields a slope of 1.00. Also shown in Figure S 5 is the reported absorption cross section from Nizkorodov et al. (2004) recorded at 596 Torr total pressure. The discrepancy between the high and low pressure data remains unknown, and was not observed in an analogous studies from (Vandaele et al., 2002; Vandaele et al., 2003).

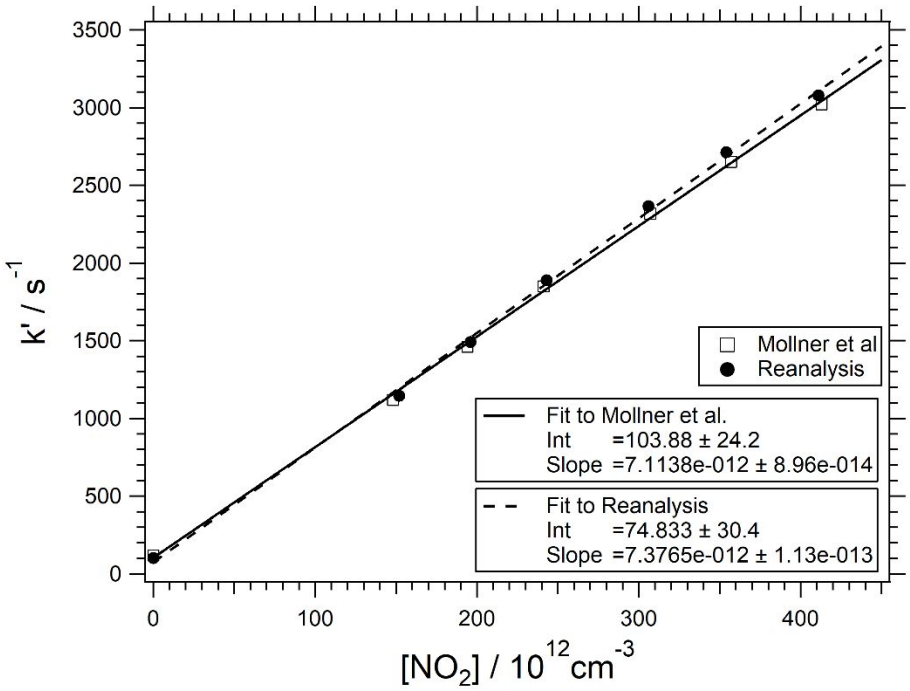


Figure S 3: Bi-molecular plot for $k_1$, measured at 200 Torr $N_2$ and 298 K from the study of Mollner et al. (2010). Raw data files were reanalyzed using the methods used in this study. Observed differences in the rate coefficients are within the uncertainty of the respective studies (±11%).

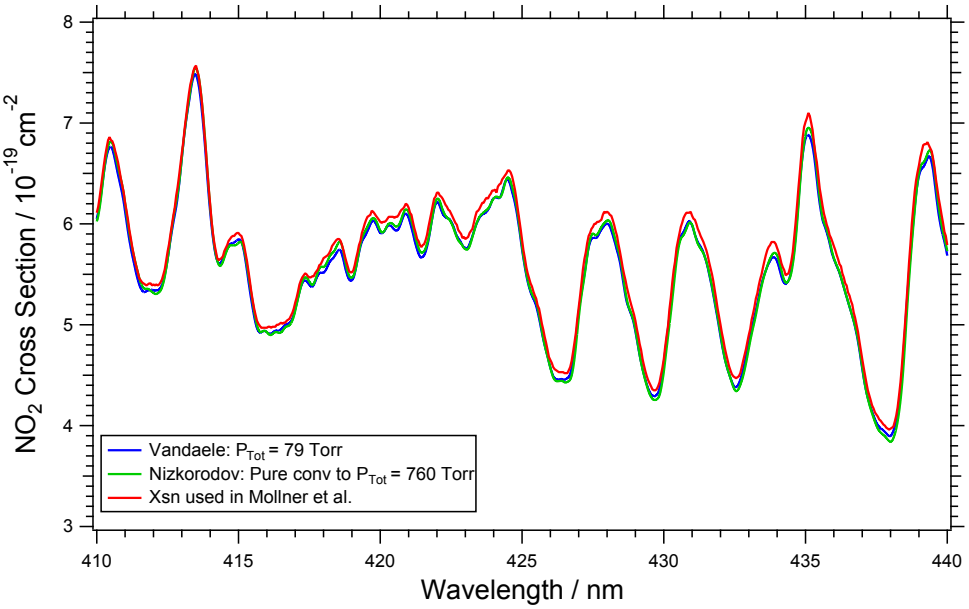


Figure S 4: Comparison of the Vandaele et al. (2002), Nizkorodov et al. (2004) $NO_2$ absorption cross sections, along with the absorption cross section for $NO_2$ used in the work by Mollner et al. (2010). Each cross section has been convolved with the ILS used in the current study (see text for details), except that of Mollner et al. (2010) which appears as observed in the analysis files. The cross section of Nizkorodov et al. (2004), recorded at 0.99 Torr, has been treated to represent the pressure broadening effect at 760 Torr (see details in text).

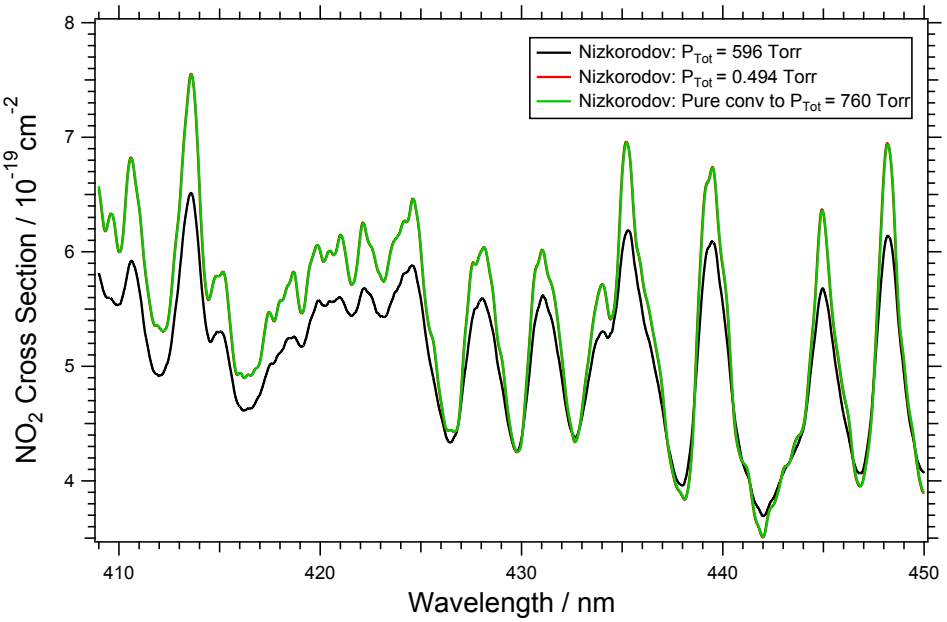


Figure S 5: Comparison of the $NO_2$ absorption cross sections reported by Nizkorodov et al. (2004), recorded at 596 and 0.494 Torr. All datasets have been convolved with the ILS used in this study. The green spectrum, has been additionally treated to represent the pressure broadening effect at 760 Torr (see details in text).

## 3 Supplementary Figures

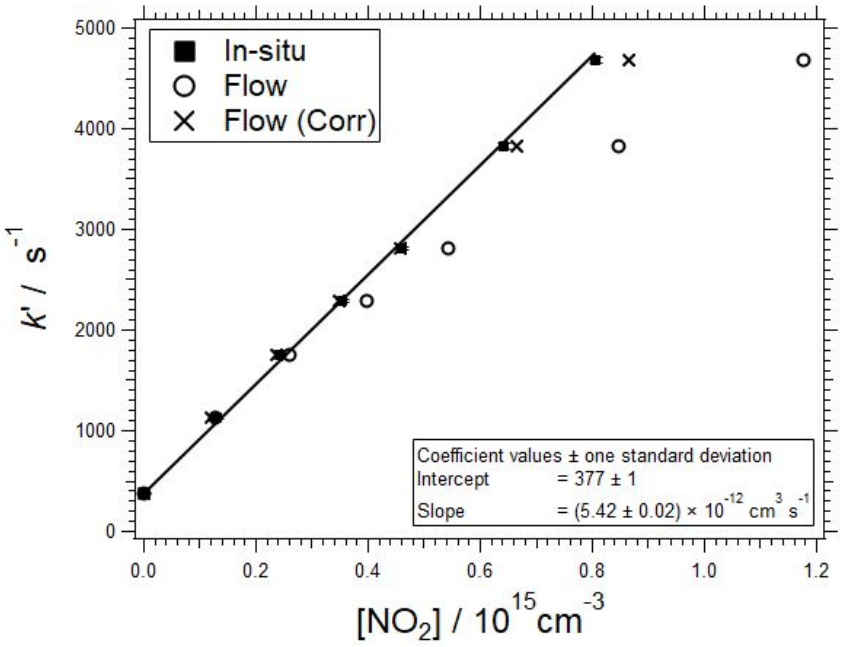


Figure S 6: Comparison of *k*' vs $[NO_2]$ for different methods of $[NO_2]$ characterization at 50 Torr $N_2$ and 230 K. Error bars in the y-axis represent the precision in the *k*' measurement to ±2σ and are shown for the "In-situ" dataset only. "In-situ" data points represent the $[NO_2]$ determined from the in-situ UV/Vis absorption axis. "Flow" data points represent $[NO_2]$ determined using the $NO_2$ pre-mix concentration (0.34%) and volumetric flow rates (0 – 90 sccm in 500 sccm total). "Flow (Corr)" is the same "Flow" data corrected for the $N_2O_4$ equilibrium concentration, based on the equilibrium constant from Burkholder et al. (2020) and $[NO_2] = \left(\sqrt{8\,[NO_2]_0\,K_{eq} + 1}\right)/4K_{eq}$. Observed curvature in "Flow" at $[NO_2] > 0.2 \times 10^{15}$ $cm^{-3}$ is primarily due to the dimerization of $NO_2$ to $N_2O_4$, however the applied correction does not resolve the discrepancy with the In-situ entirely, suggesting an additional loss of $NO_2$ or $N_2O_4$ or possible minor impurities in the $NO_2$ source.

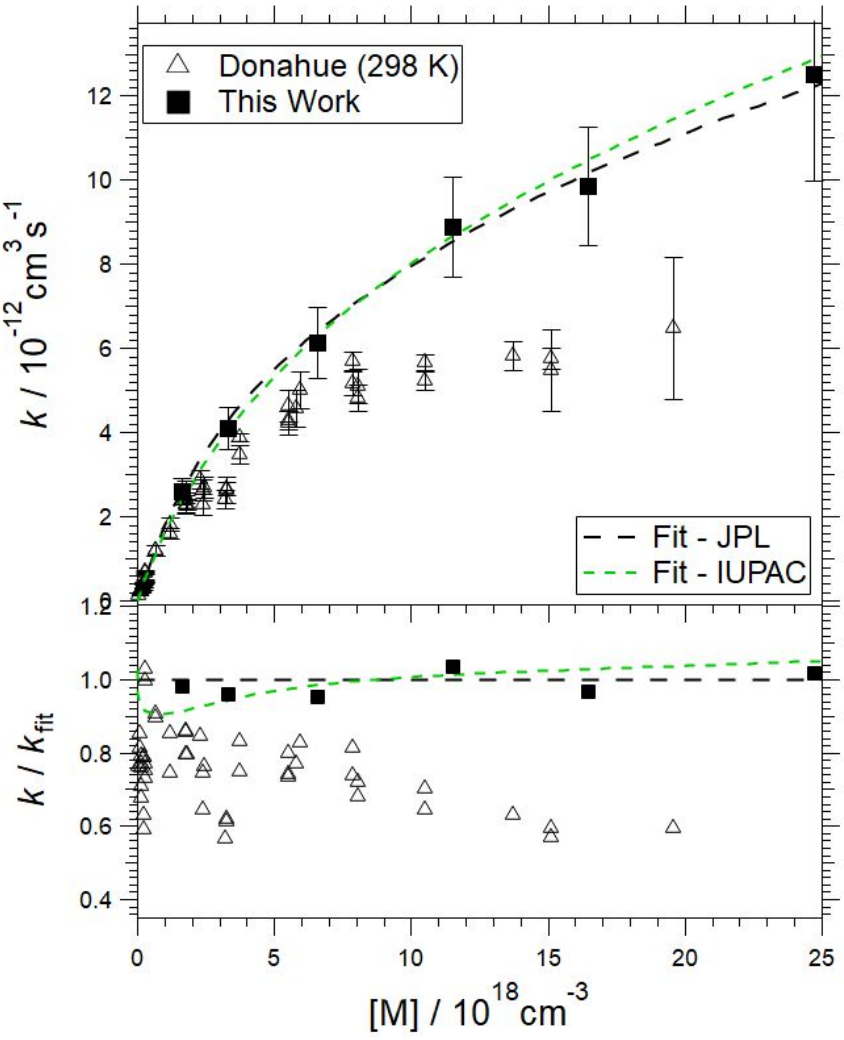


Figure S 7: The total rate constant, $k_1$, as a function of [M] ($N_2$) at 293 K compared to literature data from Donahue et al. (1997). Error bars represent the total uncertainty to 2σ. Fits to this work using the IUPAC (Atkinson et al., 2004) and JPL (Burkholder et al., 2020) fall-off parametrizations are also shown.

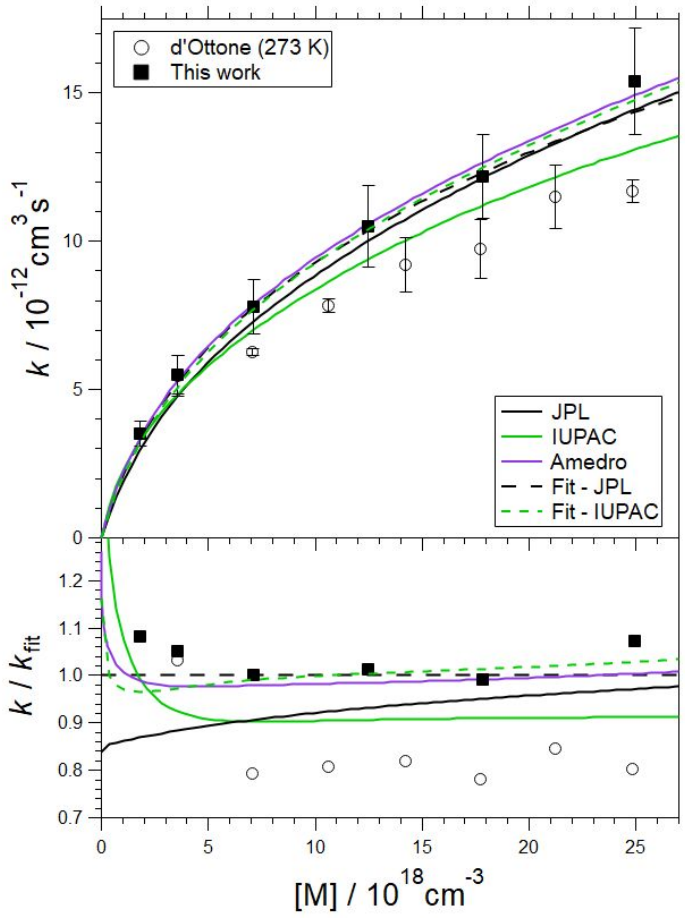


Figure S 8: The total rate constant, $k_1$, as a function of [M] ($N_2$) at 271K compared to literature data from D'Ottone et al. (2001). Error bars represent the total uncertainty to 2σ. Fits to this work using the IUPAC (Atkinson et al., 2004) and JPL (Burkholder et al., 2020) fall-off parametrizations are also shown along with the current parameterizations from JPL (Burkholder et al., 2020), IUPAC (Atkinson et al., 2004) and Amedro et al. (2019).

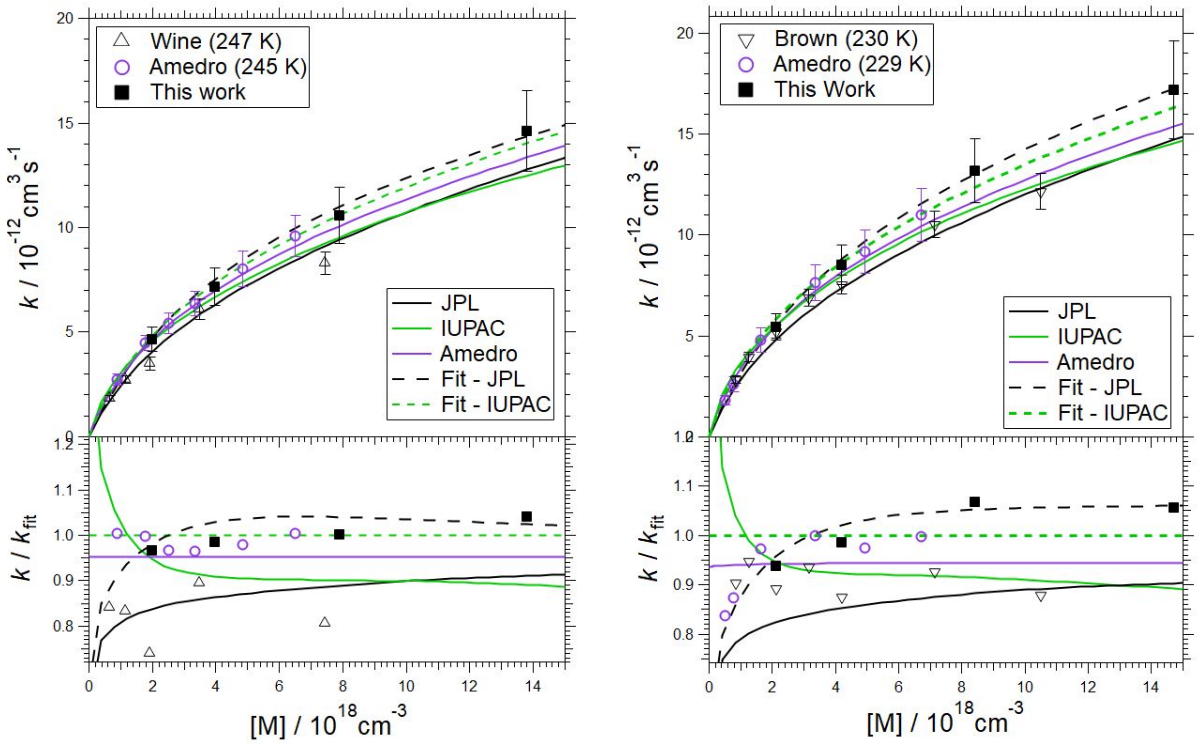


Figure S 9: Comparison of experimental data taken at 230 and 245 K with literature data from Wine et al. (1979), Brown et al. (1999) and Amedro et al. (2019). Error bars represent the total uncertainty to 2σ. Parameterizations of $k_1$ from JPL (Burkholder et al., 2020), IUPAC (Atkinson et al., 2004) and Amedro et al. (2019) are shown for comparison. $k_{fit}$ is represented by the fit to this work using the IUPAC parameterization (eq. 4, main text), in comparison to the JPL parameterization used in the main text figures.

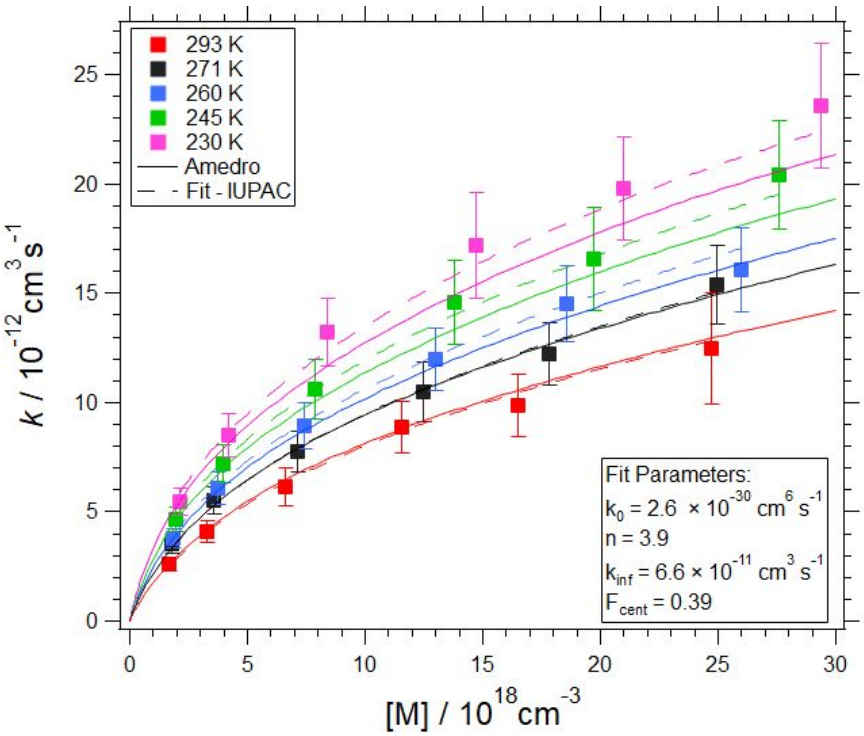


Figure S 10: Rate constant, $k_1$, for the reaction of OH + $NO_2$ as a function of [$N_2$] (p = 50 – 750 Torr) measured over range of temperatures (293 – 230 K). Data was fit with the weighted JPL recommended Troe function (Eq. 2, main text), and is compared to the predicted $k$ calculated from the recent work by Amedro et al. (2019), which uses the IUPAC parameterization with the following constants: $k_0 = 2.6 \times 10^{-30}$ cm$^6$ molecule$^{-2}$ s$^{-1}$, $k_{inf} = 6.3 \times 10^{-11}$ cm$^3$ molecule$^{-1}$ s$^{-1}$, $n$ = 3.6 and $F_{cent} = 0.39$. Error bars represent the total uncertainty in the average $k_1$ to ±2σ.

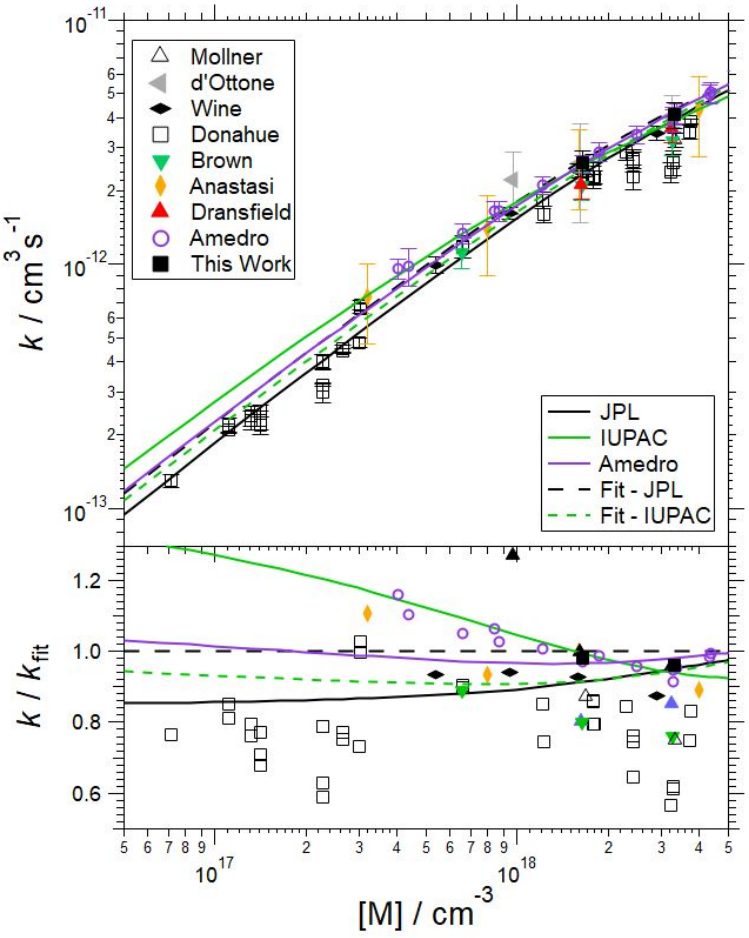


Figure S 11: Low-pressure literature data comparison at 293 K (Anastasi and Smith, 1976; Wine et al., 1979; Donahue et al., 1997; Brown et al., 1999; Dransfield et al., 1999; D'Ottone et al., 2001; Mollner et al., 2010; Amedro et al., 2019).

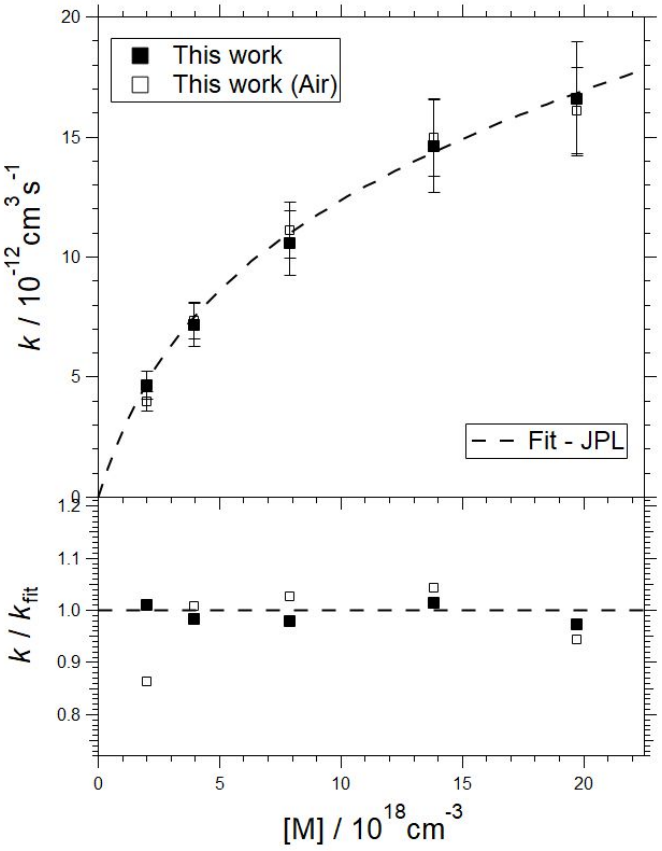


Figure S 12: The total rate constant, $k_1$, as a function of [M] at 245 K in $N_2$ and Air bath gases. Error bars represent the total uncertainty to 2σ.

## 4 References


Amedro, D., Bunkan, A. J. C., Berasategui, M., and Crowley, J. N.: Kinetics of the OH + $NO_2$ reaction: Rate coefficients (217-333 K, 16-1200 mbar) and fall-off parameters for $N_2$ and $O_2$ bath-gases, Atmos. Chem. Phys., 10643–10657, 10.5194/acp-19-10643-2019, 2019.

Anastasi, C., and Smith, I. W. M.: Rate measurements of reactions of OH by resonance absorption Part 5.-Rate constants for OH + $NO_2$(+M) → $HNO_3$(+M) over a wide range of temperature and pressure, J. Chem. Soc.. Faraday Trans. 2, 72, 1459-1468, 1976.

Atkinson, R., Baulch, D. L., Cox, R. A., Crowley, J. N., Hampson, R. F., Hynes, R. G., Jenkin, M. E., Rossi, M. J., and Troe, J.: Evaluated kinetic and photochemical data for atmospheric chemistry: Volume I - gas phase reactions of O-x, HOx, NOx and SOx species, Atmos. Chem. Phys., 4, 1461-1738, 2004.

Brown, S. S., Talukdar, R. K., and Ravishankara, A. R.: Rate constants for the reaction OH + $NO_2$ + M → $HNO_3$ + M under atmospheric conditions, Chem. Phys. Lett., 299, 277-284, 1999.

Burkholder, J. B., Sander, S. P., Abbatt, J., Barker, J. R., Cappa, C., Crounse, J. D., Dibble, T. S., Huie, R. E., Kolb, C. E., Kurylo, M. J., Orkin, V. L., Percival, C. J., Wilmouth, D. M., and Wine, P. H.: Chemical Kinetics and Photochemical Data for Use in Atmospheric Studies, Evaluation No. 19, Pasadena, 2020.

D'Ottone, L., Campuzano-Jost, P., Bauer, D., and Hynes, A. J.: A pulsed laser photolysis-pulsed laser induced fluorescence study of the kinetics of the gas-phase reaction of OH with $NO_2$, J. Phys. Chem. A, 105, 10538-10543, doi:10.1021/jp012250n, 2001.

Donahue, N. M., Dubey, M. K., Mohrschladt, R., Demerjian, K., and Anderson, J. G.: High-pressure flow study of the reactions OH + $NO_x$ → $HONO_x$: Errors in the falloff region, J. Geophys. Res., 102, 6159-6168, 1997.

Dransfield, T. J., Perkins, K. K., Donahue, N. M., Anderson, J. G., Sprengnether, M. M., and Demerjian, K.: Temperature and pressure dependent kinetics of the gas-phase reaction of the hydroxyl radical with nitrogen dioxide, Geophys. Res. Lett., 26, 687-690, 1999.

Liu, Y. D., and Sander, S. P.: Rate Constant for the OH plus CO Reaction at Low Temperatures, J. Phys. Chem. A, 119, 10060-10066, 10.1021/acs.jpca.5b07220, 2015.

Mollner, A. K., Valluvadasan, S., Feng, L., Sprague, M. K., Okumura, M., Milligan, D. B., Bloss, W. J., Sander, S. P., Martien, P. T., Harley, R. A., McCoy, A. B., and Carter, W. P. L.: Rate of gas phase association of hydroxyl radical and nitrogen dioxide, Science, 330, 646-649, doi:10.1126/science.1193030, 2010.

Nizkorodov, S. A., Sander, S. P., and Brown, L. R.: Temperature and pressure dependence of high-resolution air-broadened absorption cross sections of $NO_2$ (415-525 nm) J. Phys. Chem. A, 108, 4864-4872, doi:10.1021/jp049461n, 2004.

Vandaele, A. C., Hermans, C., Fally, S., Carleer, M., Colin, R., Mérienne, M.-F., and Jenouvrier, A.: High-resolution Fourier transform measurement of the $NO_2$ visible and near-infrared absorption cross-section: Temperature and pressure effects, J. Geophys. Res., 107, ACH 3-1 - ACH 3-12, 2002.

Vandaele, A. C., Hermans, C., Fally, S., Carleer, M., and Merienne, M.-F.: Absorption cross-sections of $NO_2$: simulation of temperature and pressure effects, J. Quant. Spectrosc. Radiat. Transfer, 76, 373-391, 2003.

Wine, P. H., Kreutter, N. M., and Ravishankara, A. R.: Flash photolysis-resonance fluorescence kinetics study of the reaction OH + $NO_2$ + M → $HNO_3$ + M, J. Phys. Chem., 83, 3191-3195, doi:10.1021/j100488a002, 1979.